ACS APPLIED MATERIALS & INTERFACES

Research Article

www.acsami.org

Facile Preparation of Hierarchical TiO_2 Nano Structures: Growth Mechanism and Enhanced Photocatalytic H_2 Production from Water Splitting Using Methanol as a Sacrificial Reagent

Zeeshan Haider and Young Soo Kang*

Korea Center for Artificial Photosynthesis and Department of Chemistry, Sogang University, Seoul 121-742, Republic of Korea

Supporting Information

ABSTRACT: Owing to unique features, hierarchical nanostructure of TiO_2 has superior photocatalytic activity. In this work a facile hydrothermal route has been explored to prepare 3D hierarchical TiO_2 (3D-HTiO$_2$), 1D/3D hybrid hierarchical TiO_2 composite (HHC), and 3D hierarchical protonated titanate microspheres $H_2Ti_2O_5{\cdot}H_2O$ (3DHPTMS) at the expense of free-standing titania nanotube membrane (TiO_2-Memb). It proceeded through the formation of peroxotitanium complex, a water-soluble Ti complex as an intermediate. Mechanism of formation, role of membrane crystallinity, and reaction parameters giving fine control on tuning morphology and crystal structure have been investigated systematically. Photocatalytic activities were determined by measuring the amount hydrogen generated from water splitting under UV irradiation in the presence of methanol as a sacrificial reagent. Self-assembled hierarchical titania nanostructures exhibited much superior photocatalytic activity compared to that of starting material, i.e., TiO_2-Memb. Enhanced photocatalytic activity is due to characteristic morphology, increased surface area, and enhanced production of photogenerated charge carriers.

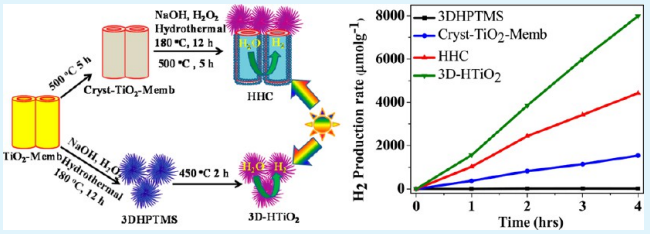

KEYWORDS: *1D/3D hybrid hierarchical TiO_2 composite, 3D hierarchical TiO_2, titania nanotubes membrane, photocatalytic water splitting, H_2 generation, peroxotitanium complex*

INTRODUCTION

Titanium dioxide (TiO_2) with wide band gap (3.2 eV) has been extensively studied for energy applications such as solar cell,[1] batteries,[2] photocatalysis,[3] CO_2 photoreduction[4] and water splitting.[5] Numerious critical factors such as extended light absorption, separation of electron and hole pairs, crystalline phase, surface area, particle size, and morphology govern the overall efficiency of these devices. Among the eight polymorph phases of TiO_2,[6] the anatase phase has the highest surface photoactivity,[7] the rutile phase is the most stable thermodynamic form,[8] and brookite is the least studied polymorph because it is difficult to prepare with phase purity.[9]

Artificial photosynthesis as emerging technology has been intensively studied for the next generation solar fuel production[10−12] Since the discovery of photocatalytic property of TiO_2 by Fujishima and Honda,[13] many studies have been devoted for photochemical as well as photoelectrochemical (PEC) water splitting for solar hydrogen production.[14] Various methodologies such as plasmonic coupling,[15] hetrostructuring,[16] band gap engineering by N and C doping,[3,5] formation of black and red TiO_2,[17−20] and crystal facet engineering[21−23] are developed to improve photocatalytic performance. Our research group has also contributed toward improved PEC performance via fabricating facet oriented photocatalytic films on conducting substrate with selective exposure of highly reactive crystal facets.[24−26] However, the water splitting efficiencies achieved so far are much less compared to theoretically predicted values because of several limiting factors such as low absorption of solar radiation and high rate of electron/hole pair recombination due to the defects and low diffusion coefficient of electron/hole in the crystals.[27] Existence of grain boundaries in particulate titania acts as carrier trapping sites.[28] One dimensional (1D) TiO_2 nanostructures such as nanotubes arrays,[29] nanorods,[30] and nanowires[31] provides direct pathway for electron transfer due to extended diffusion length.[32] One dimensional TiO_2 nanostructures can minimize the grain boundaries for the electron/hole diffusion. However, they suffer the drawback of lower surface area.[33] Hierarchically assembled one-dimensional TiO_2 structures exhibit multiple advantages such as high degree of roughness and increased surface area. These factors favor extended separation and transfer of electronic charge carriers.[34] It has been reported that branched nanorods,[35] hierarchical nanowires,[36] and nanotubes[37] of titania have shown significant improvement in photocatalytic performance. Moreover, the improvement in energy conversion efficiency by a three-dimensional urchin-like structure of TiO_2 is attributed to the high surface area and

Received: March 26, 2014
Accepted: June 17, 2014
Published: June 17, 2014

entrapment of incident radiation due to the light scattering effect.[38]

Hence, it was highly desirable to combine the advantages of both high surface area of three-dimensional (3D) TiO_2 and better electron transport properties of 1D TiO_2 due to the minimized grain boundaries to improve light harvesting and electron/hole diffusion capabilities.[39] This work is focused on the preparation of 3D hierarchical TiO_2 nanostructure (3D-HTiO_2) and 1D/3D hybrid composite (HHC) by hydrothermal transformation of anodized TiO_2 nanotubes membrane (TiO_2-Memb). Fabrication process was composed of two steps, ambient temperature etching of TiO_2-Memb in H_2O_2 solution followed by hydrothermal reaction in NaOH solution. It was accompanied by intermediate formation of protonated titanates which were transformed into TiO_2 by thermal annealing. It was found that annealing temperature of TiO_2-Memb had played an important role in controlling desirable morphology of hierarchical TiO_2 nanostructures. The TiO_2-Memb without annealing as well as with moderate annealing (below 300 °C) resulted in the complete transformation into 3D-HTiO_2. As annealing temperature of membrane was higher than or equal to 300 °C, composite structure (HHC) having both 1D and 3D TiO_2 was produced. Moreover, when the concentrations of H_2O_2 and NaOH were changed, TiO_2 nanostructures with various morphologies (nanoparticles, nanospindle and nanoplates) with the desired crystalline phase (anatase or brookite) were obtained. Photocatalytic activities of TiO_2-Memb and hierarchical TiO_2 nanostructures were studied comparatively by measuring the amount of hydrogen gas generated from water splitting. This study provides a versatile route to fabricate the hierarchical TiO_2 nanostructures with tunable morphology and crystal structure. Considering practical application of TiO_2 as photocatalyst, a significant improvement in photocatalytic water splitting efficiency has been achieved.

EXPERIMENTAL SECTION

Materials and Chemicals. Titanium foil (0.25 mm thick, 99.7% purity), ammonium fluoride (NH_4F, 98.0%), ethylene glycol ($C_2H_5O_2$, 99.8%), and hexachloroplatinic acid hexahydrate ($H_2PtCl_6{\cdot}6H_2O$, 8 wt %) were purchased from Sigma-Aldrich. Hydrogen peroxide (H_2O_2, 35%) was obtained from Jin Chemicals. Sodium hydroxide (NaOH, 97.0%) and hydrochloric acid (HCl, 35−37%) were obtained from Daejung Chemicals. All reagents were used without any further purification. Aqueous solutions were prepared using doubly distilled water (DDW) obtained from Millipore.

Preparation of TiO_2-Memb. TiO_2-Memb was prepared by electrochemical anodization of Ti foil.[40] Briefly Ti foil (2 cm × 3 cm) was washed by ultrasonication in acetone, ethanol, and DDW. Anodization was performed in ethylene glycol having 0.3 wt % ammonium fluoride and 2 vol % DDW at 60 V for 10 h using Pt foil as counter electrode. Undesired debris from the top of anodized TiO_2 nanotube arrays was removed by ultrasonication in water and ethanol. TiO_2-Memb was separated from Ti foil using methanol wetting.[41]

Preparation of Hierarchical TiO_2 Nanostructures. TiO_2-Memb (0.02 g) was aged in 2 mL of 35% H_2O_2 solution until complete etching of the entire membrane was obtained. The clear yellow solution obtained was transferred into a 30 mL Teflon-lined autoclave. A 10 mL of 0.5 M NaOH solution was added. After room temperature stirring for 30 min, autoclave was heated in electric oven at 180 °C for 12 h. White precipitates were collected by centrifuge and washed several times with DDW. Acid washing was performed by aging the above precipitates in 0.1 M HCl solution (10 mL) for 4 h. It produced 3DHPTMS, which were thermally annealed in air at 450 °C (for 2 h) to produce 3D-HTiO_2. The Cryt-TiO_2-Memb (annealed at 500 °C for 5 h) was partially etched upon aging in H_2O_2 solution. Under the identical hydrothermal conditions it produced HHC. In a similar way it was washed with dilute HCl solution and air annealing was performed at 500 °C for 5 h.

Preparation of TiO_2 Nanocrystals with Tunable Morphology and Crystalline Phase. TiO_2-Memb was completely etched in reduced amount of 35% H_2O_2 (0.2 mL). NaOH solution (10 mL) of variable concentration such as 0.01, 0.05, and 0.1 M was introduced in it, and hydrothermal reaction was carried out 180 °C for 12 h. White precipitates were recovered by centrifuge and washed several times with only DDW.

Materials Characterization. The morphologies were observed using scanning electron microscope (SEM-JSM 7600F operated at 20 keV) and transmission electron microscope (TEM-JEM 211F operated at 20 keV). Elemental composition was determined by energy-dispersive X-ray spectroscopy (EDAX) attached to SEM. XRD measurement was performed using Rigaku miniFlex-II desktop diffractometer Cu Kα radiation (λ = 0.154 056 Å) with 2θ range of 7°−60°. BET surface area and pore volume distribution were analyzed by measuring nitrogen adsorption−desorption isotherm (Autosorb-1 Quantachrome Instruments). Samples were vacuum degassed at 250 °C before measurement. Thermogravimetric analysis (TGA) was carried out using TGA thermal analyzer Scinco STAN-650 at a heating rate of 5 °C/min from room temperature to 500 °C in Ar flow. Diffused reflectance spectra were measured using a UV−visible−NIR spectrophotometer (Carry 5000). XPS survey and high resolution spectra were measured using an X-ray photoelectron spectrophotometer (Sigma Probe).

Photocatalytic Activity Measurement: Photocatalytic H_2 Evolution. Photocatalytic H_2 evolution was observed in the water/methanol mixture (v/v, 9/1), where methanol acted as a sacrificial reagent to capture photogenerated holes during photolysis. A 40 mg of photocatalyst was dispersed in mixture of water and methanol with total volume of 40 mL (catalyst to solvent ratio of 1 g/L). Photocatalytic experiment was performed in the in-house-developed cylindrical quartz photoreactor (volume capacity of 100 mL), surrounded by steel covering and fitted with quartz window for irradiation and septum to withdraw gas sample. H_2 evolution was performed with in situ photodeposition of 1% Pt by adding 10 μL of 8 wt % H_2PtCl_6 solution under continuous stirring in a top irradiation mode using 300 W Xe lamp (Max-302, Asahi Spectra, Japan) as light source set 20 cm away from the top of the reactor. The focused UV intensity measured at top of reactor using UV radiometer YK-34UV (Lutron Electronics, Taiwan) was observed as 1.8 mW/cm^2. Before irradiation the whole system was deaerated by purging with Ar gas (1 h) at a flow rate of 70 sccm controlled by mass flow controller unit (MFC). During water splitting reaction by UV irradiation, a 500 μL gas sample was withdrawn intermittently from the headspace of reactor using gastight syringe (SGE, Analytical Science, Australia) and injected manually into a gas chromatograph (GC-78790A, Aligent Technologies) equipped with thermal conductivity detector (TCD), which was operated using Ar as carrier gas. Retention time observed for H_2 gas was 2.325 min. The concentration of H_2 was calculated from pre-established calibration curve obtained from H_2 gas of known concentrations. The amount of H_2 gas was calculated using ideal gas law $PV = RT$.

RESULTS AND DISCUSSION

Morphology and Crystal Structure of 3DHPTMS. TiO_2-Memb was obtained by anodization of Ti foil by applying an external electric field followed by separating it from Ti foil. SEM image of top view (Figure 1a) indicates the uniform pore distribution with an average diameter of 90 nm. The length of the membrane was around 110 μm (Figure 1b). The TiO_2 nanotubes surface was very smooth (Figure 1c). The optical image (Figure 1d) indicates perfect delamination of TiO_2-Memb from Ti substrate. The delamination mechanism has been reported elsewhere.[40−42] XRD pattern given in the Supporting Information indicated that as formed TiO_2-Memb was amorphous in nature without appearance of any character-

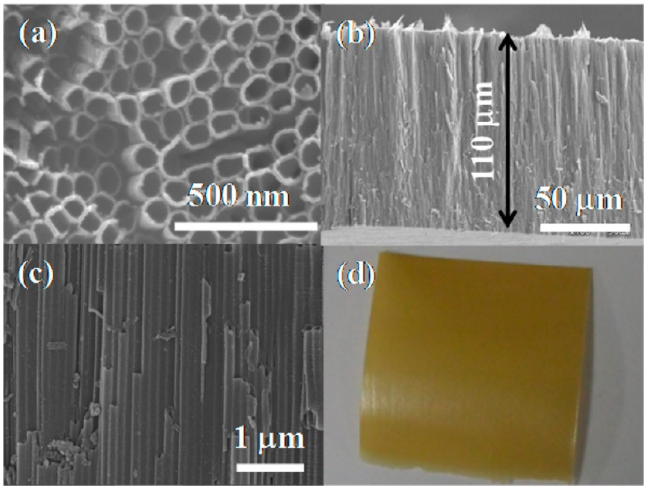

Figure 1. SEM images: top view (a), cross section (b), magnified cross view (c), and optical image (d) of TiO_2-Memb.

istic diffraction peak. Air annealing (500 °C for 5 h) produces well crystalline anatase phase of TiO_2 membrane (Cryst-TiO_2-Memb) as shown in Figure S1. Physicochemical properties of amorphous titania are entirely different from those of the crystallized form.

It is obvious that amorphous TiO_2-Memb (Figure S2a) before annealing with inferior chemical resistance is prone to be readily dissolved in H_2O_2 solution for a short period of time and it produced a clear yellow solution (Figure S2b). However, Cryst-TiO_2-Memb (Figure S2c) was partially etched in H_2O_2 solution and most part of it was settled down (Figure S2d). Appearance of yellow color is due to the formation of water-soluble peroxotitanium solution. It has been reported in literature that peroxotitanium solution can have different colors ranging from orange to pale yellow.

It is related to existence of different forms of the peroxotitanium complex such as cationic $[Ti(O_2)(OH)_3]^+$, uncharged $[Ti(O_2)(OH)_3]$, or anionic $[Ti(O_2)(OH)_3]^-$ depending upon solution pH.[43,44] The pH of TiO_2-Memb etched solution was measured as 1.04, which indicates the formation of neutral form of peroxotitanium complex. In general, titanium chloride ($TiCl_4$) is most commonly used for making peroxotitanium solution. However, chlorides can adversely affect electrical characteristics.[45] Peroxotitanium solution derived from TiO_2-Memb does not involve chlorides. Ti-complex solution was completely transformed into uniformly dispersed 3D hierarchical spheres. SEM image (Figure 2a) of hydrothermal reaction product indicated the formation of 3D urchin-like morphology. Absence of any trace impurity of TiO_2-Memb ensured the complete transformation. TEM analysis (Figure 2b,c) indicates that the hierarchical spheres with diameter around 900 nm are constructed by self-assembly of large number of two-dimensional nanoplates as building block material. The width of 2D nanoplates was around 5 nm (Figure 2d). The Ti complex so formed does not hold enough stability. During hydrothermal treatment it decomposed and reacted with alkaline species present in the reaction medium.

XRD pattern (Figure S3b) confirmed the formation of sodium titanate microspheres (3D-NaTMS). Washing with dilute HCl solution resulted in the formation of 3DHPTMS, which was confirmed by XRD pattern (Figure 3c). The appearance of diffraction peaks at 2θ values of 9.7°, 24.6°, 39°, and 48.4° were indexed to the lattice planes (200), (110),

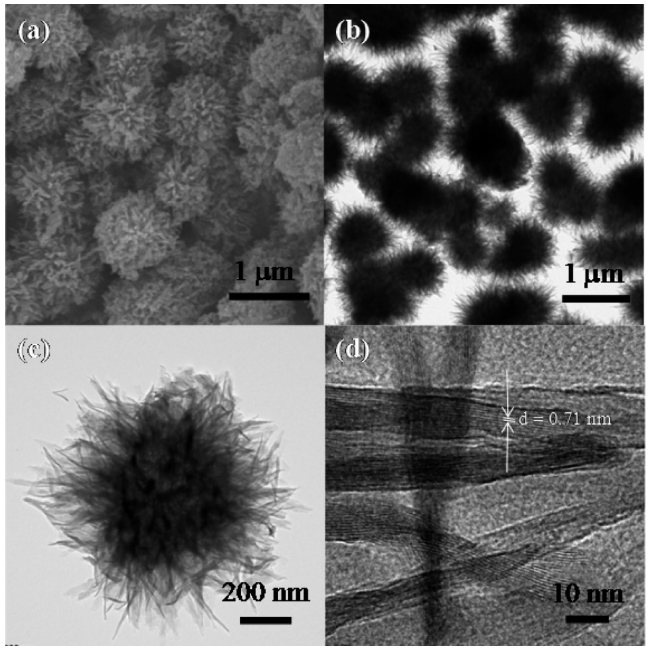

Figure 2. SEM image (a), TEM images (b, c), and HRTEM image (d) of 3DHPTMS obtained from 0.5 M NaOH and 2 mL of H_2O_2 using TiO_2-Memb (without preannealing).

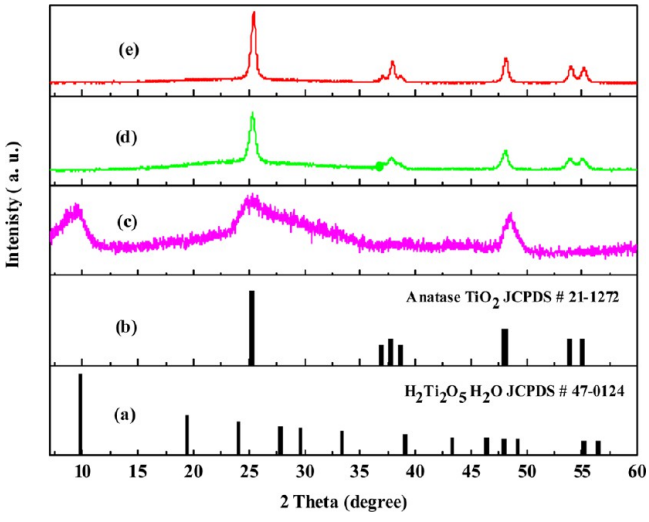

Figure 3. XRD patterns of reference $H_2Ti_2O_5{\cdot}H_2O$, JCPDS no. 47-0124 (a), reference peaks of anatase TiO_2 JCPDS no. 21-1272 (b), 3DHPTMS (c), 3D-HTTiO_2 (d), and HHC (e).

(501), and (020) of the orthorhombic phase of $H_2Ti_2O_5{\cdot}H_2O$ (JCPDS no. 47-0124).[46] The interlayer spacing (0.71 Å) measured by HRTEM (Figure 2d) also confirmed the formation of hydrogen titanate. A shift in the peak position of (200) and (310) planes (Figure S3) is due to the difference in the ionic radius between Na^+ and H^+ intercalated in the interlayer spacing of lepidocrocite titantes.[47] Complete replacement of Na^+ with H^+ was ensured from energy dispersive X-ray (EDAX) spectrum given in the Figure S4.

Effect of Concentration (H_2O_2 and NaOH) on Morphology of 3DHPTMS. Concentration of hydrogen peroxide and NaOH can be varied to control the size and morphology of 3DHPTMS as summarized in Figure 4. To evaluate individual role of hydrogen peroxide and NaOH, the

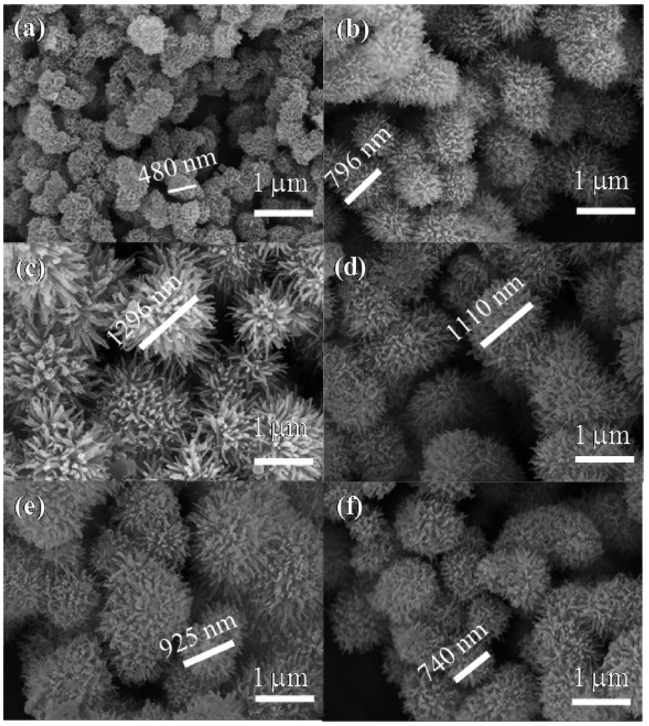

Figure 4. SEM images of 3DHPTMS using 2 mL of H_2O_2 with varied concentrations of NaOH of 0.1 M (a), 0.3 M (b), 1.0 M (c) and at 0.5 M NaOH with varied amounts of H_2O_2 solution of 1 mL (d), 3 mL (e), and 5 mL (f).

concentration of one reactant was increased gradually while keeping the other constant. When the NaOH concentration was increased, a gradual increase in diameter of 3DHPTMS was observed. A 0.1 M NaOH solution gave hierarchical spheres with an average diameter of 480 nm, whereas the increase of NaOH concentration to 0.3 and 1.0 M produced hierarchical spheres with an average diameter of 796 and 1296 nm, respectively. In addition to the size variation, packing density of hierarchical spheres was also influenced by alkali concentration. A lower concentration produced self-assembled hierarchical spheres in loosely packed form, while an increase in alkali concentration produced densely packed spheres having urchin-like morphology with the existence of many side branches (Figure 4a–c).

It appears that size and morphology of 3DHPTMS are critically dependent on concentration of NaOH as well as H_2O_2. Sutradhar et al. has reported an inverse relationship between NH_4OH concentration and corresponding size of TiO_2 spheres.[48] However, this study reveals that size of 3DHPTMS was increased with increasing NaOH concentration. Such phenomenon is based on pH dependent variation in growth kinetics of hierarchical spheres. Peroxotitanium complex is reported to have high stability under acidic conditions.[44] Extended stability means unfavorable conditions for release of titanium from stable complex. However, as solution pH is increased, peroxotitanium complex undergoes deprotonation and its stability is reduced.[44] At higher pH value titanium is likely to be released more easily from the complex and sodium titanate nuclei will grow more rapidly. It is due to direct influence of NaOH concentration on growth kinetics of sodium titanate that 1.0 M NaOH produced hierarchical spheres of much bigger in size compared to that of 0.1M. Similar trials were conducted to vary the amount of H_2O_2 at fixed concentration of NaOH (0.5 M). In contrast to the effect of alkali concentration on the size of hierarchical TiO_2 spheres, increasing the amount of H_2O_2 solution behaved strikingly in the opposite way. As in Figure (4d–f) the increasing amount of H_2O_2 solution resulted in the decreased size of hierarchical spheres. H_2O_2 as a stabilizing agent can control the hydrolysis rate of peroxotitanium solution. Excess of H_2O_2 can suppress the growth rate of hierarchical spheres. Hence, a decrease in the size of hierarchical spheres was observed with higher concentration of H_2O_2. However, morphology of hierarchical spheres was quite close to each other and variation in the size was also less pronounced compared to variable concentration of NaOH solution.

Formation Mechanism of 3DHPTMS. At room temperature, TiO_2-Memb etching in H_2O_2 medium accompanied by formation of water-soluble peroxotitanium complex $[Ti(O_2)(OH)_3]$ is indicated in eq 1. Being unstable, the so formed Ti-complex can be easily hydrolyzed into titanic acid (eq 2). However, such an undesirable reaction can be prevented by the use of excess of H_2O_2 as indicated by eq 3.[43] During hydrothermal reaction in the presence of NaOH solution the complex of $[Ti(O_2)(OH)_3]$ was thermally decomposed to produce sodium titanate as shown by eq 4. A large number of nuclei assemble together to produce sodium titanate nanocrystals and result in a spherical shape to favor surface energy minimization.[49] Acid washing resulted in the replacement of Na^+ by H^+ through simple ion exchange process, and 3DHPTMS was produced (eq 5).[47]

$$Ti^{4+} + H_2O_2 + 3H_2O \rightarrow [Ti(O_2)(OH)_3] + 5H^+ \quad (1)$$

$$[Ti(O_2)(OH)_3] + H_2O \rightarrow Ti(OH)_4 + \frac{1}{2}O_2 + OH^- \quad (2)$$

$$Ti(OH)_4 + H_2O_2 \rightarrow [Ti(O_2)(OH)_3] + H_3O^+ \quad (3)$$

$$4[Ti(O_2)(OH)_3] + 4NaOH \rightarrow 2Na_2Ti_2O_5\cdot H_2O + 6H_2O + 3O_2 \quad (4)$$

$$Na_2Ti_2O_5\cdot H_2O + 2HCl \rightarrow H_2Ti_2O_5\cdot H_2O + NaCl \quad (5)$$

$$H_2Ti_2O_5\cdot H_2O \rightarrow 2TiO_2 + 2H_2O \quad (6)$$

Formation of 3D-HTiO$_2$. Thermal annealing in air (450 °C for 2 h) transformed 3DHPTMS into 3D-HTiO$_2$.[48] XRD pattern (Figure 3d) confirmed the appearance of anatase phase of TiO_2.

SEM and TEM images (Figure 5a,b) indicate the formation of spherical nanocrystals with retention of hierarchical morphology. Electron diffraction pattern (Figure 5c) shows that 3D-HTiO$_2$ were well crystallized. During annealing, phase

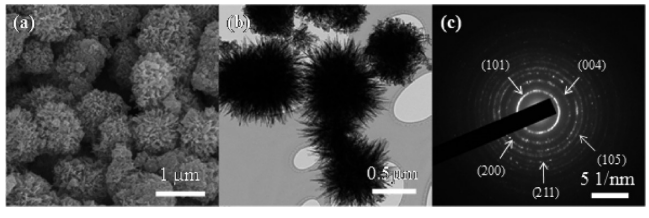

Figure 5. SEM image (a), TEM image (b), and electron diffraction pattern (c) of 3D-HTiO$_2$ obtained from 0.5 M NaOH and 2 mL of H_2O_2.

transition is related to dehydration of 3DHPTMS as represented by eq 6.[48] It was monitored by thermogravimetric analysis (Figure 6). As the weight loss of 13.12% was observed

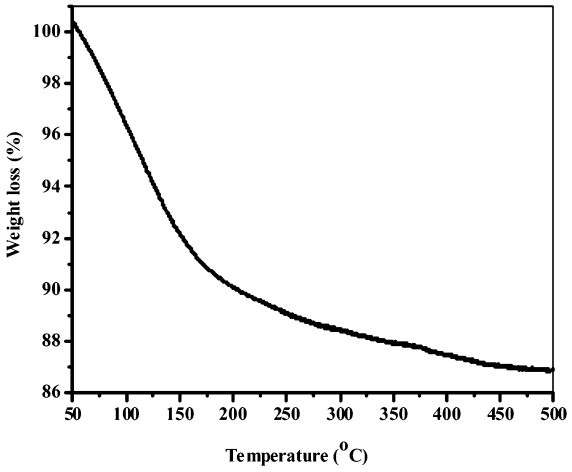

Figure 6. TGA data of as-prepared 3DHPTMS during heating in Ar flow.

up to 500 °C, such loss is due to the removal of physically adsorbed water as well as dehydration of protonated titanates.[50] Effect of concentration on size variation of 3D-HTiO$_2$ is summarized in Supporting Information Figure S5.

N$_2$ Adsorption/Desorption Isotherms and BET Surface Area Measurement. Mesoporous nature of 3DHPTMS and 3D-HTiO$_2$ was analyzed by nitrogen adsorption/desorption isotherm curves shown in Figure 7. The specific surface area

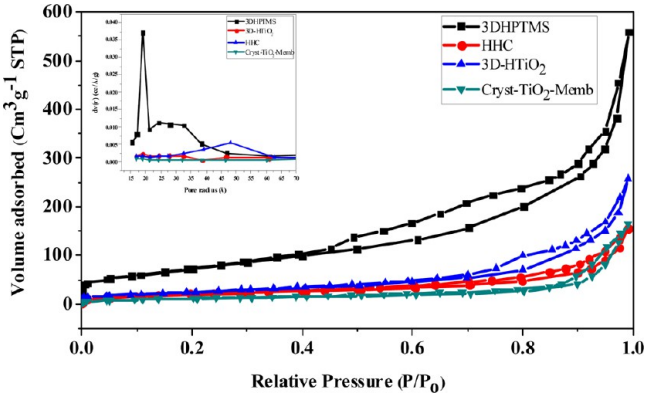

Figure 7. N$_2$ adsorption/desorption isotherms of TiO$_2$-Memb, 3DHPTMS, 3D-HTiO$_2$, HHC and corresponding pore size distribution profiles (given in inset).

was measured by Brunauer–Emmet–Teller (BET) method, while pore size distribution was determined from pore volume distribution curves (given in the inset of Figure 7) by applying Barrett–Joyener–Halenda (BJH) method.

The calculated specific surface area and total pore volume of 3DHPTMS were observed as 303.6 m^2 g^{-1} and 0.70 cm^3 g^{-1}, respectively. However, its transformation into 3D-HTiO$_2$ by air annealing was accompanied by decrease in the surface area and total pore volume up to 97.7 m^2 g^{-1} and 0.20 cm^3 g^{-1}, respectively. The observed surface area and total pore volume of 3D-HTiO$_2$ are still higher compared to those of Cryst-TiO$_2$-Memb as 41.6 m^2 g^{-1} and 0.22 cm^3 g^{-1}. Such an increase in the specific surface area as well as mesoporous nature of hierarchical titania is highly desirable to achieve significant improvement in photocatalytic performance.

Formation of HHC. Cryst-TiO$_2$-Memb was partially etched in H_2O_2 solution even after several hours of aging. Limited dissolution of Cryst-TiO$_2$-Memb in H_2O_2 solution is quite obvious because of increase in chemical resistance owing to higher crystallinity. Hydrothermal treatment and postannealing transformed Cryst-TiO$_2$-Memb into HHC. The HHC was composed of both 3D-hierachical spheres as well as 1D-hierarchical TiO$_2$ nanostructures. A small fraction of Cryst-TiO$_2$-Memb etched in H_2O_2 solution produced 3D-hierachical spheres, whereas the major fraction of Cryst-TiO$_2$-Memb being undissolved in H_2O_2 solution was transformed into 1D-hierarchical TiO$_2$ nanostructures. From the SEM (Figure 1c) and TEM images (Figure 8b,c) it is apparent that sidewalls of

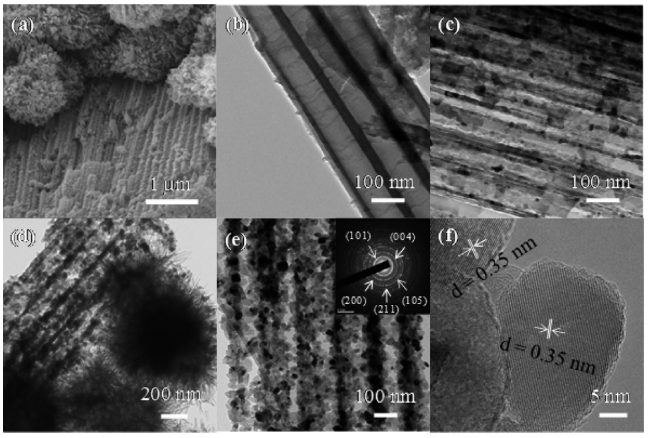

Figure 8. SEM and TEM image of TiO$_2$-Memb (a, b), TEM images of Cryst-TiO$_2$-Memb (c), and TEM image (d, e) and HRTEM image (f) of HHC, obtained from 0.5 M NaOH and 2 mL of H_2O_2 using Cryst-TiO$_2$-Memb (preannealing at 500 °C, 5 h).

TiO$_2$-Memb were smooth in appearance. Hydrothermal transformation produced HHC. Coexistence of 3D-hierachical spheres and 1D-hierarchical TiO$_2$ nanostructures is evident from Figure 8a,d,e. XRD pattern (Figure 3e) confirmed the formation of single crystalline anatase phase of TiO$_2$. Very interestingly during hydrothermal formation of HHC the smooth walls of TiO$_2$-Memb were homogeneously transformed into 1D-hierarchical TiO$_2$.

A large number of crystallites (diameter of ~50 nm) appeared to be attached on the side walls. The electron diffraction pattern (inset of Figure 8e) and HRTEM image (Figure 8f) indicated their crystal structure as anatase phase of TiO$_2$. The HHC has a high surface roughness. It was responsible for the increase in the specific surface area. The surface area of HHC was observed as 60.21 m^2 g^{-1}, which is much higher compared to those of TiO$_2$-Memb as 41.6 m^2 g^{-1}. Such fabrication of large surface area morphology can enhance the surface adsorption of reactants during photocatalytic reactions. Very recently Ye et al. has fabricated 1D hierarchical TiO$_2$ photoanode. They demonstrated significant improvement in PCE efficiency of DSSC.[51] However, this work is focused on transformation of TiO$_2$-Memb into 3D hierarchical and 1D/3D hybrid hierarchical composite of TiO$_2$ under controlled experimental conditions as well as exploring their application to photocatalytic hydrogen production via water splitting reaction in the presence of methanol as a sacrificial reagent.

Effect of Membrane Preannealing Temperature on the Formation of HHC. TiO_2-Memb was air annealed at different temperatures before hydrothermal reaction to figure out the possible influence of preannealing temperature on the formation of HHC. The product obtained from TiO_2-Memb annealed at 200 °C was quite similar to that obtained from amorphous membrane in terms of complete transformation into 3DHPTMS during hydrothermal reaction (Figure 9a).

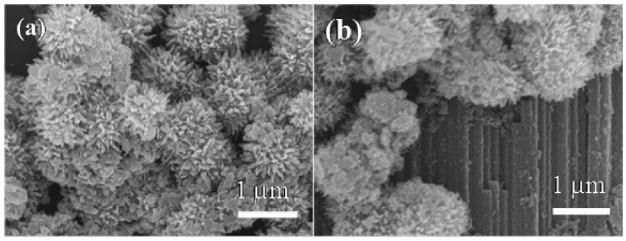

Figure 9. SEM image of hydrothermal products obtained from Cryst-TiO_2-Memb preannealed at 200 °C, 5 h (a) and at 300 °C, 5 h (b), with 0.5 M NaOH and 2 mL of H_2O_2.

However, as the preannealing temperature was raised to 300 °C, it produced composite structure having both 3D-hierarchical spheres and 1D-hierachcial TiO_2 nanostructure (Figure 9(b)).

It is noteworthy that earlier reports in literature have exploited the difference in crystallinity between the closed bottoms and side walls of TiO_2-Memb for selective opening of bottoms to get through hole free-standing TiO_2-Memb.[42] However, to the best of our knowledge, the fabrication of hierarchical composite by controlling crystallinity of TiO_2-Memb has not been realized, as highlighted in this work. The procedure mentioned in this work is not simply an alternative route to make peroxotitanium solution. Rather it describes crystallinity controlled partial or complete etching of TiO_2-Memb. This can be helpful for fabricating titania based composites as well as nanoscale heterostructures for desirable applications. Ultimate objective of this work is significant enhancement in the photoactivity of TiO_2-Memb as expected because of increased surface area and formation of hierarchical TiO_2 nanostructures.

Fluorine and Carbon Doping. Fluorine and carbon elements can possibly be incorporated to TiO_2-Memb by anodization in fluorinated organic electrolyte.[52,53] Presence of carbon on the surface of TiO_2 can enhance photoreactivity,[54] whereas fluorine is reported to have suppressive role.[55] Elemental composition was determined by XPS analysis. Survey spectra of TiO_2-Memb (Figure S6a) indicated the appearance of sharp peaks at 37.5, 62.5, 284.5, 459, 530, 564, 685, and 975 eV which represent the binding energies of Ti 3p, Ti 3s, C 1s, Ti 2p, O 1s, Ti 2s, F 1s, and OKLL respectively.[56,57] Figure S6b shows the Ti 2p spectrum. The two peaks at 464.5 and 458.7 eV were assigned to Ti $2p_{1/2}$ and Ti $2p_{3/2}$, respectively.[53] Four peaks were observed for O 1s spectra (Figure S6c) at positions of 533.5, 532.4, 531.3, and 530.1 eV, which correspond to the binding energies of water molecules, chemically adsorbed oxygen, hydroxyl group, and Ti−O bonds, respectively.[58] Figure S6d shows the C 1s spectrum. Three characteristic peaks of C1S at 284.5, 285.9, and 288.5 eV were observed. The peak at 284.5 eV is assigned to carbon present in all XPS measurements. The peak at 285.9 eV was assigned to T−C−O bonds. It indicates the presence of interstitial carbon in TiO_2, whereas the peak at 288.5 eV was due to surface adsorbed oxidized carbon C═O.[59] F 1s spectra (Figure S6(e)) indicated a sharp peak at 684.4 eV. This reflected physically adsorbed F atoms on the surface of TiO_2.[52] Figure 10a shows the peak intensities of F 1s of different samples.

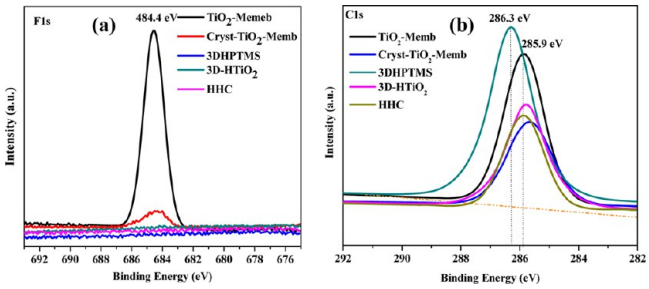

Figure 10. F 1s spectra (a) and C 1s (b) of TiO_2-Memb, 3DHPTMs, and hierarchical TiO_2 nanostructures.

It appeared that F as dopant was present in TiO_2-Memb. However, the intensity of F 1s was decreased significantly by annealing.[55] Similar reduction of peak intensity was observed for 3DHPTMS and hierarchical TiO_2 nanostructures due to possible elimination of F during hydrothermal processing. In contrast to F, the C was detected in all samples (Figure 10b). A slight shift in binding energy of C 1s was observed for 3DHPTMS compared to that of various structures of TiO_2.

Optical Absorption Characteristics. Figure S7 shows UV−visible diffused reflectance spectra of TiO_2-Memb, Cryst-TiO_2-Memb, 3DHPTMS, and hierarchical TiO_2 nanostructures. Extending absorption observed in the range of approximately 400−450 was attributed to carbon doping as observed from the XPS analysis (Figures S6d and 10b). Band gap (E_g) was determined from Tauc plot given in Supporting Information (Figure S8). E_g values of TiO_2-Memb, Cryst-TiO_2-Memb, 3DHPTMS, 3D-$HTiO_2$, and HHC were observed as 3.05, 3.1, 3.29, 3.17, and 3.15 eV, respectively. The observed red shift in absorption onset is due to the presence of carbon as dopant.

Tuning Morphology and Crystalline Phase of TiO_2 Nanostructures. Varying the concentration of H_2O_2 and NaOH provided valuable tool to prepare TiO_2 nanocrystals with tunable shape as well as crystal structure. As discussed above for 20 mg of TiO_2-Memb, the amount of H_2O_2 as low as 2.0 mL and NaOH concentration as low 0.5 M were enough to produce 3D-$HTiO_2$ with intermediate formation of 3DHPTMS. Further increase in either H_2O_2 amount or NaOH concentration just changed the size and packing density of hierarchical spheres as in Figure 4. However, working with very little amount of H_2O_2 as 0.2 mL, TiO_2 nanocrystals with diverse morphologies were obtained as a function of gradual increase in NaOH concentration (Figure 11). Control of crystal structure as either anatase or brookite phase of TiO_2 was also possible without going through intermediate formation of hydrogen titanate (Figure 12). Hydrothermal reaction of only peroxotitanium complex solution without using any NaOH produced nanoparticles of diameter of around 50 nm (not shown here). Nanoparticles with identical morphology were obtained while using very dilute (0.01 M) solution of NaOH as shown in Figure 11a,b. Corresponding XRD patterns (Figure 12d) indicated the formation of anatase phase of TiO_2. The

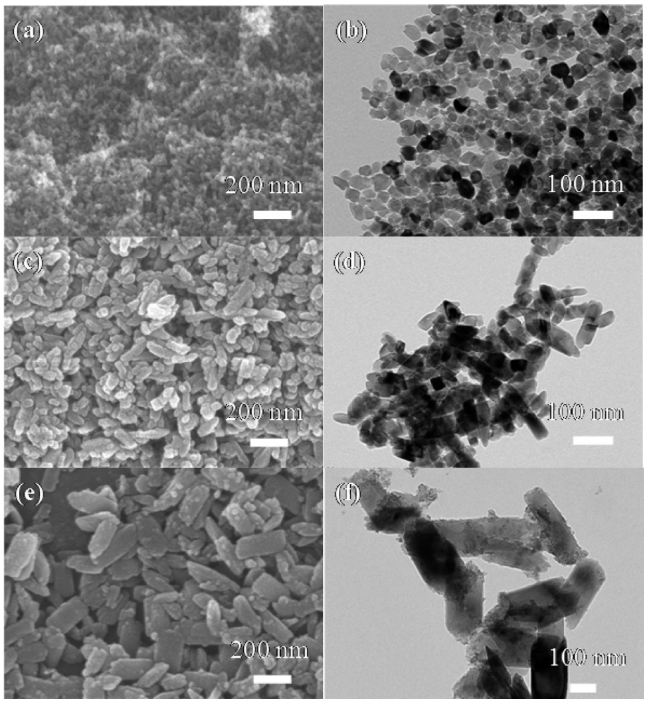

Figure 11. SEM and TEM images of titania: nanoparticles, nanospindles, and nanoplates obtained from TiO_2-Memb using 0.2 mL of H_2O_2 with varying concentrations of NaOH of 0.01 M (a, b), 0.05 M (c, d), and 0.1 M (e, f).

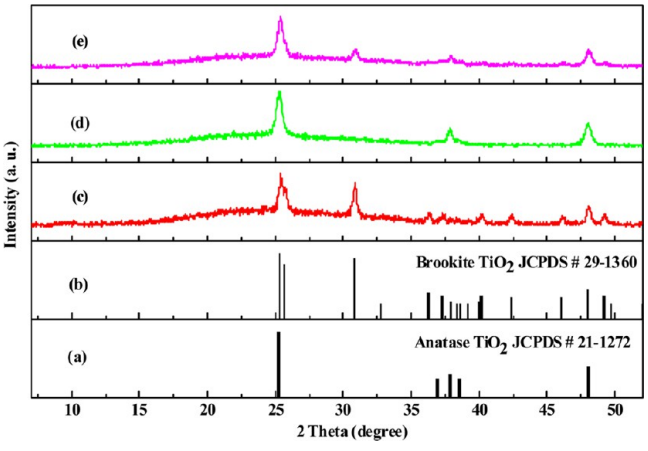

Figure 12. XRD patterns: reference peaks of anatase TiO_2 (a) and brookite TiO_2 (b) and various morphologies of TiO_2 of nanoplates (c), nanoparticles (d), and nanospindles (e).

diffraction peaks match well to the standard pattern of anatase (JCPDS no. 21-1272) given in Figure 12a.

Increase of NaOH concentration to 0.05 M produced spindle shaped titania (Figure 11c,d), the average length of which was around 100 nm, and it appeared to have mixed anatase and brookite phase of TiO_2 (Figure 12e).

Further increase of NaOH concentration up to 0.1 M resulted in production of TiO_2 nanoplates (Figure 11e,f) with an average length of 200 nm. These nanoplates were identified as single crystalline brookite phase of TiO_2 (Figure 12c). The diffraction peaks match well to the standard pattern of brookite (JCPDS no. 29-1360) given in Figure 12b.

The above discussion highlights that, in addition to TiO_2-Memb crystallinity, the choice of appropriate concentration (both H_2O_2 and NaOH) is essential to prepare hierarchical TiO_2 nanostructure with desirable morphology as well as crystalline phase. Fabrication of various morphologies is highlighted by schematic illustration given in Figure 13. It is

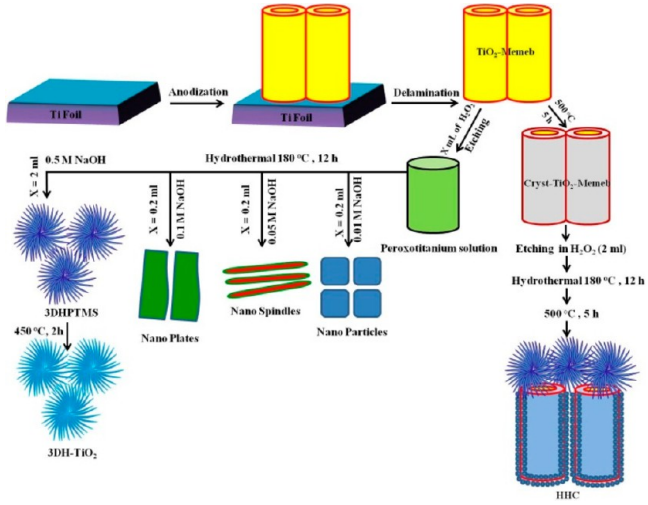

Figure 13. Schematic diagram for fabrication of 3DHPTMS, 3D-HTiO_2, HHC, and various morphologies from hydrothermal transformation of TiO_2-Memb.

important to note that very low concentration of NaOH (0.01 M) produced anatase phase of TiO_2 and that medium concentration of NaOH (0.05 M) gave the mixed phase of anatase and brookite while high concentration of NaOH (0.1 M) resulted in the formation of single crystalline brookite phase of TiO_2. Such observation is consistent with a recent report describing that formation of brookite phase of TiO_2 is highly favored at higher pH.[9]

Photocatalytic H_2 Generation by Water Splitting. During photocatalytic reaction a nanoscale hierarchical TiO_2 can reduce the recombination of photogenerated electron and hole pairs, as they can be efficiently utilized before getting diffused. Similarly, the increase in roughness and surface area can extend the number of active sites. Integration of these factors into one unit of photocatalysts could possibly favor superior photoactivities. In order to testify such an assumption, hierarchical TiO_2 nanostructures as well as Cryst-TiO_2-Memb were tested for photocatalytic H_2 production through water splitting under UV irradiation in the presence of methanol as a sacrificial reagent. For the sake of comparison under similar conditions the Cryst-TiO_2-Memb was milled into powder form prior to BET and H_2 test. By being milled, Cryst-TiO_2-Memb was transformed into smaller fragments as shown in Figure S9. Time dependent production of H_2 and corresponding rate of H_2 production are given in Figure 14. The average H_2 production observed by Cryst-TiO_2-Memb was 385 μmol h^{-1} g^{-1}. The HHC and 3D-HTiO_2 produced 661 and 1310 μmol $h^{-1}g^{-1}$, respectively, which are 1.72 and 3.4 times higher than that of Cryst-TiO_2-Memb. Such an improvement in the water splitting efficiency is attributed to corresponding increase in the surface area as well as better utilization of charge carriers. Increase in the surface area of hierarchical TiO_2 nanostructures can promote better dispersion and higher loading of Pt nanoparticles during photodeposition process. This may be another factor to the increase in corresponding rate of H_2 production. The H_2 production rate of various samples and

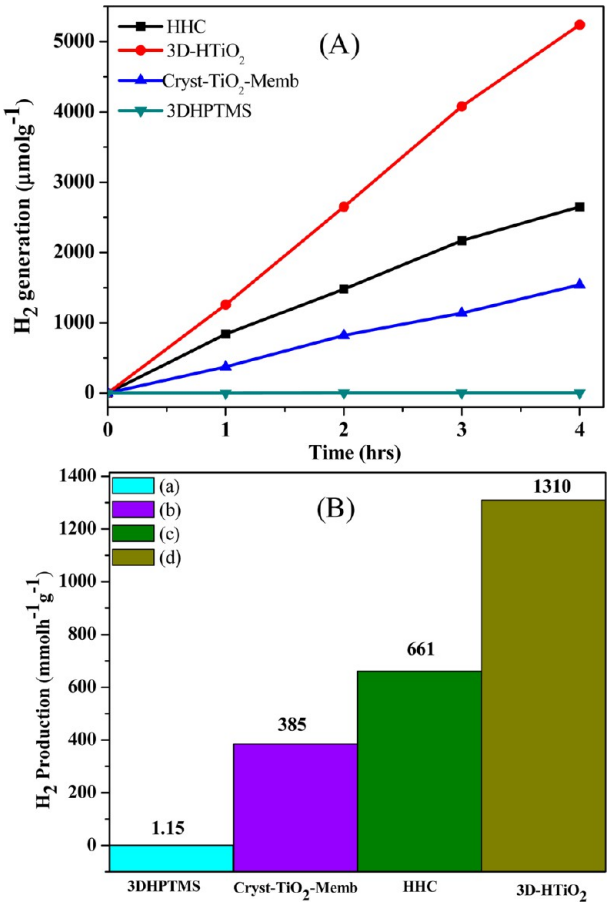

Figure 14. Time course for H_2 production (A) and corresponding rate (B) of 1% Pt deposited 3DHPTMS, Cryst-TiO_2-Memb (500 °C, 5 h), HHC, and 3D-$HTiO_2$, obtained from 0.5 M NaOH and 2 mL of H_2O_2.

corresponding BET surface areas are summarized in Table 1. Among various samples, 3DHPTMS occupies the highest

Table 1. Comparison of Photocatalytic H_2 Production Rates and Corresponding BET Surface Areas of Cryst-TiO_2-Memb (Preannealed at 500 °C, 5 h), 3DHPTMS, 3D-$HTiO_2$, and HHC

sample	H_2 production rate (μmol h^{-1} g^{-1})	BET surface area (m^2 g^{-1})
Cryst-TiO_2-Memb	385	41.6
HHC	661	60.21
3D-$HTiO_2$	1310	97.7
3DHPTMS	1.15	303.6

surface area at 303.6 m^2 g^{-1}. However, it expressed the least H_2 generation (1.15 μmol h^{-1} g^{-1}). Because of much difference in measurement conditions of hydrogen evolution as reported in literature, it is not easy to directly compare H_2 generation observed in this work with reported values. However, titanate nanotubes have been reported to have very low values of H_2 evolution from water splitting.[60] The important reasons of less activity of 3DHPTMS can be related to poor crystallinity (Figure 3c), larger band gap (Figure S8c),[61] and shorter lifetime of photogenerated charge carriers.[34]

Presence of residual trace of sodium may also adversely affect photocatalytic activity.[62,63] It would be appropriate to consider that instead of any single parameter, multiple factors such as surface area, morphology, crystallinity, crystalline phase, absorption band, and lifetime of separated electron are playing a critical role while governing overall photoactivity.

As mentioned above, the transformation of TiO_2-Memb into hierarchical TiO_2 nanostructures significantly enhanced the amount of H_2 generation. Among various samples, 3D-$HTiO_2$ showed the highest improvement; as observed, it was 3.4 times higher than that of TiO_2-Memeb. However, the given rate of H_2 production does not represent the optimized one. Tuning appropriate size of 3DHPTMS and 3D-$HTiO_2$ and adjusting relative proportion of 1D and 3D constituents of HHC could possibly make further improvement in H_2 generation. To figure it out, nanoparticles of 3DHPTMS and 3D-$HTiO_2$ with different size were examined for H_2 production under similar testing conditions. As is clear from the SEM images (Figure S5), 3D-$HTiO_2$ increases in size by increasing NaOH concentration.

Figure 15 shows that H_2 production rate was influenced by the corresponding size of 3D-$HTiO_2$. The sample prepared with the lowest NaOH concentration (i.e., 0.1 M) has the highest H_2 production with an observed value of 1996 μmol h^{-1} g^{-1}, which is 5.18 times higher than that of the starting material of Cryst-TiO_2-Memb.

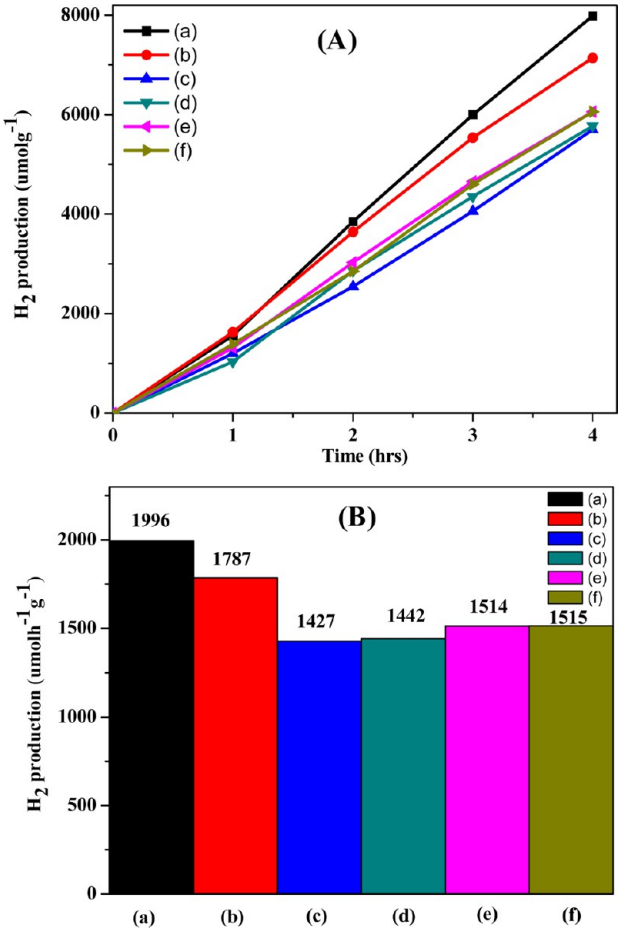

Figure 15. Time course for H_2 production (A) and corresponding rate (B) of 1% Pt deposited 3D-$HTiO_2$ obtained from varied concentrations of NaOH and H_2O_2 volume of 0.1 M, 2 mL (a), 0.3 M, 2 mL (b), 1.0 M, 2 mL (c), 0.5 M, 1 mL (d), 0.5 M, 3 mL (e), and 0.5 M, 5 mL (f).

dx.doi.org/10.1021/am501796m | ACS Appl. Mater. Interfaces 2014, 6, 10342−10352

It has been reported in the literature that NaOH concentration can markedly influence surface area, photodegradation rate, and phase transition behavior of $H_2Ti_2O_5 \cdot nH_2O$.[62] In contrast, varying the concentration of H_2O_2 during formation of peroxotitanium solution resulted in a slight modification in corresponding H_2 production (Figure 15). 3DHPTMS was also studied to explore size dependent H_2 production. However, compared to 3D-HTiO_2, it expressed very low activity (Figure S10). As explained earlier, the entirely different behavior toward H_2 production is related to intrinsic electronic and optical characteristics of 3DHPTMS.

The impact of preannealing of Cryst-TiO_2-Memb on corresponding rate of H_2 production is summarized in Figure 16. Since annealing temperature of TiO_2-Memb controls

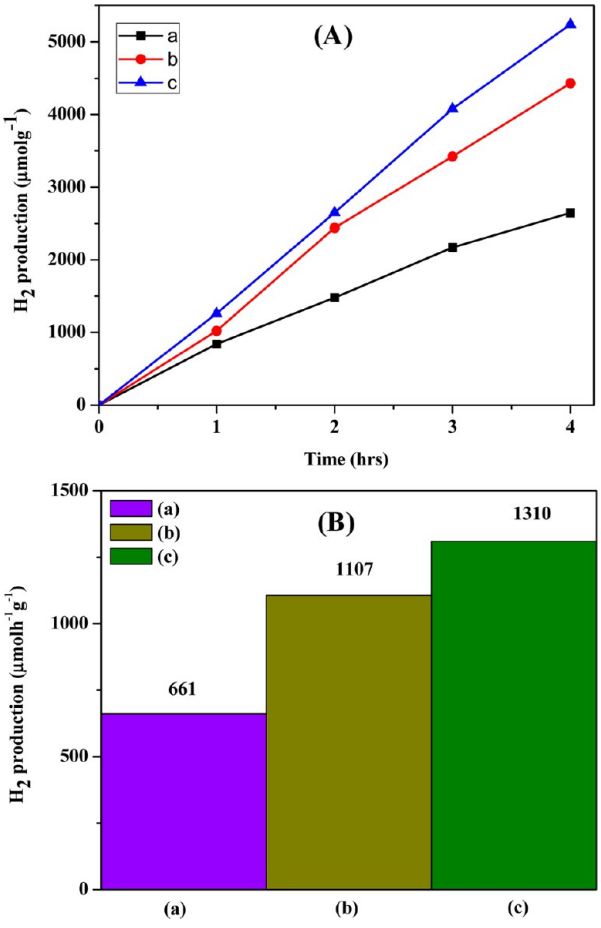

Figure 16. Time course for H_2 production (A) and corresponding rate (B) of 1% Pt deposited HHC and 3D-HTiO_2 obtained from 0.5 M NaOH and 2 mL of H_2O_2, with different preannealed TiO_2-Memb at 500 °C, 5 h (a) and 300 °C, 5 h (b) and without preannealing (c).

dissolution rate during etching in H_2O_2 solution, it can influence on relative proportion of 1D and 3D constituents of HHC during hydrothermal reaction (Figure 5, Figure 8, and Figure 9). H_2 evolution rates observed for HHC samples preannealed at 500 and 300 °C were observed as 661 and 1107 μmol h^{-1} g^{-1}, respectively, whereas without preannealing TiO_2-Memb was absolutely transformed into 3D-HTiO_2 instead of HHC, producing even higher rate of H_2 generation such as 1310 μmol h^{-1} g^{-1} as shown in Figure 14B and Figure 16B. It is generalized that a decrease in preannealing temperature of TiO_2-Memb (before hydrothermal treatment) increases the corresponding rate of H_2 production. Figure 7 and Table 1 show that BET surface area of 3D-HTiO_2 (97.7 m^2 g^{-1}) is much higher than that of 1D TiO_2-Memb counterpart (41.6 m^2 g^{-1}). Higher H_2 production is due to more favorable etching of TiO_2-Memb in H_2O_2 solution producing higher proportion of 3D component of HHC, which thereby contributes to relatively higher surface area, and hence, the increased H_2 production is observed. In this study methanol was used for H_2 production during photocatalytic water splitting. During water splitting reaction, photogenerated charge carriers on the surface of TiO_2 exhibit ultrafast recombination tendency. Existing studies in literature have revealed that recombination of photo generated carriers occur in the range of femtosecond to picoseconds time regime.[64] In order to suppress such recombination and to observe the half reaction, i.e., H_2 production, different sacrificial reagents (hole scavengers or electron donors) are frequently used. The use of methanol as the most common sacrificial reagent for H_2 production is well reported in literature.[17,54,55,60,65] However, in this study, to figure out the role of sacrificial reagent, H_2 production tests were also performed in the absence of methanol. In such a case, no measurable gas was detected by GC under similar chromatographic configuration. (Table S1). This observation is consistent with the previous studies reporting that aqueous suspension of TiO_2 could not split water.[65] Hence, the role of methanol is vital for suppressing charge carrier recombination with simultaneous boosting in H_2 production. Uncertainty was existing in the literature regarding the role of methanol as a hole scavenger or re-forming during H_2 production from water splitting. A recent finding aimed at exploring mechanistic aspect of water splitting suggests its role as sacrificial reagent. With the help of using isotopically labeled (D_2O) and (CD_3OD), it revealed that H_2 production in the presence of methanol is mainly from water splitting reaction.[66] The above discussion supports that in this study nonobservance of H_2 production in the absence of methanol is due to the high rate of carrier recombination, while its presence reduces recombination in favor of H_2 production from water splitting.

CONCLUSION

In summary, hierarchical TiO_2 nanostructures have been fabricated by transformation of TiO_2-Memb through a simple strategy. A two-step approach was based on peroxide etching of membrane at ambient conditions and hydrothermal treatment in NaOH solution. The preannealing of TiO_2-Memb was exploited to fabricate hierarchical TiO_2 with desirable morphologies. Transformation of TiO_2-Memb into hierarchical TiO_2 reflected a large increase in the specific area. The hierarchical TiO_2 exhibited excellent performance toward photocatalytic water splitting. A 5.18-fold increase in the rate of H_2 production was observed compared to that of TiO_2-Memb. Fabrication of different morphologies of TiO_2 such as nanoparticles, nanospindles, and nanoplates with adjustable crystalline phase as pure anatase or brookite was also demonstrated. Simplified strategy reported in this work can be applied to fabricate hierarchically structured other metal oxide composites, and nanoscale heterostructuring of TiO_2–metal oxides.

ASSOCIATED CONTENT

Supporting Information

XRD patterns of TiO_2-Memb and Cryst-TiO_2-Memeb, optical images of their etching in H_2O_2 solution, XRD patterns and

EDAX analysis of 3DHPTMS before and after acid washing, SEM images of various sized 3D-HTiO$_2$, XPS spectrum, UV−visible diffused reflectance spectrum, Tauc plots, band gaps curves, SEM images of milled TiO$_2$-Memb, H_2 evolution without using sacrificial reagent, and H_2 production curves of various sized 3DHPTMS. This material is available free of charge via the Internet at http://pubs.acs.org.

AUTHOR INFORMATION

Corresponding Author

*E-mail: yskang@sogang.ac.kr.

Notes

The authors declare no competing financial interest.

ACKNOWLEDGMENTS

This work was supported by the Korea Center for Artificial Photosynthesis (KCAP) located at Sogang University funded by Ministry of Education, Science, and Technology (MEST) through National Research Foundation of Korea (Grant No. 2009-0093885).

REFERENCES

(1) Sauvage, F.; Fonzo, F. D.; Bassi, A. L.; Casari, C. S.; Russo, V.; Divitini, G.; Ducati, C.; Bottani, C. E.; Comte, P.; Graetzel, M. Hierarchical TiO$_2$ Photoanode for Dye-Sensitized Solar Cells. *Nano Lett.* **2010**, *10*, 2562−2567.

(2) Bi, Z.; Paranthaman, M. P.; Guo, B.; Unocic, R. R.; Meyer, H. M.; Bridges, C. A.; Sun, X. G.; Dai, S. High Performance Cr, N-Codoped Mesoporous TiO$_2$ Microspheres for Lithium-Ion Batteries. *J. Mater. Chem. A* **2014**, *2*, 1818−1824.

(3) Asahi, R.; Morikawa, T.; Ohwaki, T.; Aoki, K.; Taga, Y. Visible-Light Photocatalysis in Nitrogen-Doped Titanium Oxides. *Science* **2001**, *293*, 269−271.

(4) Wang, W. N.; An, W. J.; Ramalingam, B.; Mukherjee, S.; Niedzwiedzki, D. M.; Gangopadhyay, S.; Biswas, P. Size and Structure Matter: Enhanced CO$_2$ Photoreduction Efficiency by Size-Resolved Ultrafine Pt Nanoparticles on TiO$_2$ Single Crystals. *J. Am. Chem. Soc.* **2012**, *134*, 11276−11281.

(5) Khan, S. U. M.; Al-Shahry, M.; Ingler, W. B., Jr. Efficient Photochemical Water Splitting by a Chemically Modified n-TiO$_2$. *Science* **2002**, *297*, 2243−2245.

(6) Kavan, L.; Gratzel, M.; Gilbert, S. E.; Klemenz, C.; Scheel, H. J. Electrochemical and Photoelectrochemical Investigation of Single-Crystal Anatase. *J. Am. Chem. Soc.* **1996**, *118*, 6716−6723.

(7) Chen, X.; Mao, S. S. Titanium Dioxide Nanomaterials: Synthesis, Properties, Modifications, and Applications. *Chem. Rev.* **2007**, *107*, 2891−2959.

(8) Lan, T.; Liu, Y.; Dou, J.; Hong, Z.; Wei, M. Hierarchically Porous TiO$_2$ Microspheres as a High Performance Anode for Lithium-Ion Batteries. *J. Mater. Chem. A* **2014**, *2*, 1102−1106.

(9) Li, K.; Xu, J.; Shi, W.; Wang, Y.; Peng, T. Synthesis of Size Controllable and Thermally Stable Rice-like Brookite Titania and Its Application as a Scattering Layer for Nano-Sized Titania Film-Based Dye-Sensitized Solar Cells. *J. Mater. Chem. A* **2014**, *2*, 1886−1896.

(10) Ampelli, C.; Centi, G.; Passalacqua, R.; Perathoner, S. Synthesis of Solar Fuels by a Novel Photoelectrocatalytic Approach. *Energy Environ. Sci.* **2010**, *3*, 292−301.

(11) Tachibana, Y.; Vayssieres, L.; Durrant, J. R. Artificial Photosynthesis for Solar Water-Splitting. *Nat. Photonics* **2012**, *6*, 511−518.

(12) Arai, T.; Sato, S.; Kajino, T.; Morikawa, T. Solar CO$_2$ Reduction Using H$_2$O by a Semiconductor/Metal-Complex Hybrid Photocatalyst: Enhanced Efficiency and Demonstration of a Wireless System Using SrTiO$_3$ Photoanodes. *Energy Environ. Sci.* **2013**, *6*, 1274−1282.

(13) Fujishima, A.; Honda, K. Electrochemical Photolysis of Water at a Semiconductor Electrode. *Nature* **1972**, *238*, 37−38.

(14) Chen, X.; Shen, S.; Guo, L.; Mao, S. S. Semiconductor-Based Photocatalytic Hydrogen Generation. *Chem. Rev.* **2010**, *110*, 6503−6570.

(15) Mubeen, S.; Lee, J.; Singh, N.; Kramer, S.; Stucky, G. D.; Moskovits, M. An Autonomous Photosynthetic Device in Which All Charge Carriers Derive from Surface Plasmons. *Nat. Nanotechnol.* **2013**, *8*, 247−251.

(16) Liu, C.; Tang, J.; Chen, H. M.; Liu, B.; Yang, P. A Fully Integrated Nanosystem of Semiconductor Nanowires for Direct Solar Water Splitting. *Nano Lett.* **2013**, *13*, 2989−2992.

(17) Lin, T.; Yang, C.; Wang, Z.; Yin, H.; Lu, X. J.; Huang, F.; Lin, J.; Xie, X.; Jiang, M. Effective Nonmetal Incorporation in Black Titania with Enhanced Solar Energy Utilization. *Energy Environ. Sci.* **2014**, *7*, 967−972.

(18) Chen, X.; Liu, L.; Yu, P. Y.; Mao, S. S. Increasing Solar Absorption for Photocatalysis with Black Hydrogenated Titanium Dioxide Nanocrystals. *Science* **2011**, *331*, 746−750.

(19) Wang, Z.; Yang, C.; Lin, T.; Yin, H.; Chen, P.; Wan, D.; Xu, F.; Huang, F.; Lin, J.; Xie, X.; Jiang, M. Visible-Light Photocatalytic, Solar Thermal and Photoelectrochemical Properties of Aluminium-Reduced Black Titania. *Energy Environ. Sci.* **2013**, *6*, 3007−3014.

(20) Liu, G.; Yin, L. C.; Wang, J.; Niu, P.; Zhen, C.; Xie, Y.; Cheng, H. M. A Red Anatase TiO$_2$ Photocatalyst for Solar Energy Conversion. *Energy Environ. Sci.* **2012**, *5*, 9603−9610.

(21) Yang, H. G.; Sun, C. H.; Qiao, S. Z.; Zou, J.; Liu, G.; Smith, S. C.; Cheng, H. M.; Lu, G. Q. Anatase TiO$_2$ Single Crystals with a Large Percentage of Reactive Facets. *Nature* **2008**, *453*, 638−641.

(22) Liu, G.; Yu, J. C.; Lu, G. Q.; Cheng, H. M. Crystal Facet Engineering of Semiconductor Photocatalysts: Motivations, Advances and Unique Properties. *Chem. Commun.* **2011**, *47*, 6763−6783.

(23) Roy, N.; Sohn, Y.; Pradhan, D. Synergy of Low-Energy {101} and High-Energy {001} TiO$_2$ Crystal Facets for Enhanced Photocatalysis. *ACS Nano* **2013**, *7*, 2532−2540.

(24) Cha, H. G.; Song, J.; Kim, H. S.; Shin, W.; Yoon, K. B.; Kang, Y. S. Facile Preparation of Fe$_2$O$_3$ Thin Film with Photoelectrochemical Properties. *Chem. Commun.* **2011**, *47*, 2441−2443.

(25) Van, T. K.; Nguyen, C. K.; Kang, Y. S. Axis-Oriented, Continuous Anatase Titania Films with Exposed Reactive {100} Facets. *Chem. Eur. J.* **2013**, *19*, 9376−9380.

(26) Zheng, J. Y.; Song, G.; Kim, C. W.; Kang, Y. S. Fabrication of (001)-Oriented Monoclinic WO$_3$ Films on FTO Substrates. *Nanoscale* **2013**, *5*, 5279−5282.

(27) Osterloh, F. E. Inorganic Nanostructures for Photoelectrochemical and Photocatalytic Water Splitting. *Chem. Soc. Rev.* **2013**, *42*, 2294−2320.

(28) Liao, J. Y.; He, J. W.; Xu, H.; Kuang, D. B.; Su, C. Y. Effect of TiO$_2$ Morphology on Photovoltaic Performance of Dye-Sensitized Solar Cells: Nanoparticles, Nanofibers, Hierarchical Spheres and Ellipsoid Spheres. *J. Mater. Chem.* **2012**, *22*, 7910−7918.

(29) Ye, M.; Xin, X.; Lin, C.; Lin, Z. High Efficiency Dye-Sensitized Solar Cells Based on Hierarchically Structured Nanotubes. *Nano Lett.* **2011**, *11*, 3214−3220.

(30) Wolcott, A.; Smith, W. A.; Kuykendall, T. R.; Zhao, Y.; Zhang, J. Z. Photoelectrochemical Water Splitting Using Dense and Aligned TiO$_2$ Nanorod Arrays. *Small* **2009**, *5*, 104−111.

(31) Hwang, Y. J.; Hahn, C.; Liu, B.; Yang, P. Photoelectrochemical Properties of TiO$_2$ Nanowire Arrays: A Study of the Dependence on Length and Atomic Layer Deposition Coating. *ACS Nano* **2012**, *6*, 5060−5069.

(32) Kongkanand, A.; Tvrdy, K.; Takechi, K.; Kuno, M.; Kamat, P. V. Quantum Dot Solar Cells. Tuning Photoresponse through Size and Shape Control of CdSe-TiO$_2$ Architecture. *J. Am. Chem. Soc.* **2008**, *130*, 4007−4015.

(33) Lv, M.; Zheng, D.; Ye, M.; Sun, L.; Xiao, J.; Guo, W.; Lin, C. Densely Aligned Rutile TiO$_2$ Nanorod Arrays with High Surface Area for Efficient Dye-Sensitized Solar Cells. *Nanoscale* **2012**, *4*, 5872−5879.

(34) Wu, W. Q.; Rao, H. S.; Xu, Y. F.; Wang, Y. F.; Su, C. Y.; Kuang, D. B. Hierarchical Oriented Anatase TiO$_2$ Nanostructure Arrays on

Flexible Substrate for Efficient Dye-Sensitized Solar Cells. *Sci. Rep.* **2013**, *3*, 1892.
(35) Cho, I. S.; Chen, Z.; Forman, A. J.; Kim, D. R.; Rao, P. M.; Jaramillo, T. F.; Zheng, X. Branched TiO_2 Nanorods for Photoelectrochemical Hydrogen Production. *Nano Lett.* **2011**, *11*, 4978−4984.
(36) Shi, J.; Hara, Y.; Sun, C.; Anderson, M. A.; Wang, X. Three-Dimensional High-Density Hierarchical Nanowire Architecture for High-Performance Photoelectrochemical Electrodes. *Nano Lett.* **2011**, *11*, 3413−3419.
(37) Yip, C. T.; Huang, H.; Zhou, L.; Xie, K.; Wang, Y.; Feng, T.; Li, J.; Tam, W. Y. Direct and Seamless Coupling of TiO_2 Nanotube Photonic Crystal to Dye-Sensitized Solar Cell: A Single-Step Approach. *Adv. Mater.* **2011**, *23*, 5624−5628.
(38) Gao, Z.; Wu, Z.; Li, X.; Chang, J.; Wu, D.; Ma, P.; Xu, F.; Gao, S.; Jiang, K. Application of Hierarchical TiO_2 Spheres as Scattering Layer for Enhanced Photovoltaic Performance in Dye Sensitized Solar Cell. *CrystEngComm* **2013**, *15*, 3351−3358.
(39) Sun, Z.; Kim, J. H.; Zhao, Y.; Attard, D.; Dou, S. X. Morphology Controllable 1D-3D Nanostructrued TiO_2 Bilayer Photoanodes for Dye Sensitized Solar Cells. *Chem. Commun.* **2013**, *49*, 966−968.
(40) Wang, J.; Lin, Z. Freestanding TiO_2 Nanotube Arrays with Ultrahigh Aspect Ratio via Electrochemical Anodization. *Chem. Mater.* **2008**, *20*, 1257−1261.
(41) Ali, G.; Yoo, S. H.; Kum, J. M.; Kim, Y. N.; Cho, S. O. A Novel Route to Large-Scale and Robust Free-Standing TiO_2 Nanotube Membranes Based on N_2 Gas Blowing Combined with Methanol Wetting. *Nanotechnology* **2011**, *22*, 245602.
(42) Chen, Q.; Xu, D. Large-Scale, Noncurling, and Free-Standing Crystallized TiO_2 Nanotube Arrays for Dye-Sensitized Solar Cells. *J. Phys. Chem. C* **2009**, *113*, 6310−6314.
(43) Kakihana, M.; Kobayashi, M.; Tomita, K.; Petrykin, V. Application of Water-Soluble Titanium Complexes as Precursors for Synthesis of Titanium-Containing Oxides via Aqueous Solution Processes. *Bull. Chem. Soc. Jpn.* **2010**, *83*, 1285−1308.
(44) Muhlebach, J.; Muller, K.; Schwarzenbach, G. The Peroxo Complexes of Titanium. *Inorg. Chem.* **1970**, *9*, 2381−2390.
(45) Camargo, E. R.; Kakihana, M. Peroxide-Based Route Free from Halides for the Synthesis of Lead Titanate Powder. *Chem. Mater.* **2001**, *13*, 1181−1184.
(46) Sutradhar, N.; Sinhamahapatra, A.; Pahari, S. K.; Bajaj, H. C.; Panda, A. B. Room Temperature Synthesis of Protonated Layered Titanate Sheets Using Peroxo Titanium Carbonate Complex Solution. *Chem. Commun.* **2011**, *47*, 7731−7733.
(47) Liu, B.; Boercker, J. E.; Aydil, E. S. Oriented Single Crystalline Titanium Dioxide Nanowires. *Nanotechnology* **2008**, *19*, 505604.
(48) Sutradhar, N.; Pahari, S. K.; Jayachandran, M.; Stepha, A. M.; Nair, J. R.; Subramania, B.; Bajaj, H. C.; Mody, H. M.; Panda, A. B. Organic Free low Temperature Direct Synthesis of Hierarhical Protonated Layered Titanates/Anatase TiO_2 Hollow Spheres and Their Task Specific Applications. *J. Mater. Chem. A* **2013**, *1*, 9122−9131.
(49) Chen, D.; Caruso, R. A. Recent Progress in the Synthesis of Spherical Titania Nanostructures and Their Applications. *Adv. Funct. Mater.* **2013**, *23*, 1356−1374.
(50) Gao, T.; Fjeld, H.; Fjellvag, H.; Norby, T.; Norby, P. In Situ Studies of Structural Stability and Proton Conductivity of Titanate Nanotubes. *Energy Environ. Sci.* **2009**, *2*, 517−523.
(51) Ye, M.; Zheng, D.; Lv, M.; Chen, C.; Lin, C.; Lin, Z. Hierarchically Structured Nanotubes for Highly Efficient Dye-Sensitized Solar Cells. *Adv. Mater.* **2013**, *25*, 3039−3044.
(52) Li, Q.; Shang, J. K. Self-Organized Nitrogen and Fluorine Co-Doped Titanium Oxide Nanotube Arrays with Enhanced Visible Light Photocatalytic Performance. *Environ. Sci. Technol.* **2009**, *43*, 8923−8929.
(53) Sreekantan, S.; Saharudin, K. A.; Lockman, Z.; Tzu, T. W. Fast-Rate Formation of TiO_2 Nanotube Arrays in an Organic Bath and Their Applications in Photocatalysis. *Nanotechnology* **2010**, *21*, 365603.
(54) Liu, B.; Liu, L. M.; Lang, X. F.; Wang, H. Y.; Wen, L. X.; Aydil, E. S. Doping High-Surface-Area Mesoporous TiO_2 Microspheres with Carbonate for Visible Light Hydrogen Production. *Energy Environ. Sci.* **2014**, DOI: 10.1039/C4EE00472H.
(55) Pan, J.; Liu, G.; Lu, G. Q.; Cheng, H. M. On the True Photoreactivity Order of {001}, {010}, and {101} Facets of Anatase TiO_2 Crystals. *Angew. Chem., Int. Ed.* **2011**, *50*, 2133−2137.
(56) He, H.; Xiao, P.; Zhou, M.; Liu, F.; Yu, S.; Qiao, L.; Zhang, Y. PtNi Alloy Nanoparticles Supported on Carbon-Doped TiO_2 Nanotube Arrays for Photo-Assisted Methanol Oxidation. *Electrochim. Acta* **2013**, *88*, 782−789.
(57) Wang, M.; Sun, L.; Lin, Z.; Cai, J.; Xie, K.; Lin, C. p-n Heterojunction Photoelectrodes Composed of Cu_2O-Loaded TiO_2 Nanotube Arrays with Enhanced Photoelectrochemical and Photoelectrocatalytic Activities. *Energy Environ. Sci.* **2013**, *6*, 1211−1220.
(58) Su, Y.; Zhang, X.; Zhou, M.; Han, S.; Lei, L. Preparation of High Efficient Photoelectrode of N-F-Codoped TiO_2 Nanotubes. *J. Photochem. Photobiol., A* **2008**, *194*, 152−160.
(59) Zhao, Y.; Li, Y.; Wang, C. W.; Wang, J.; Wang, X. Q.; Pan, Z. W.; Dong, C.; Zhou, F. Carbon-Doped Anatase TiO_2 Nanotube Array/Glass and Its Enhanced Photocatalytic Activity under Solar Light. *Solid State Sci.* **2013**, *15*, 53−59.
(60) Dang, H.; Dong, X.; Dong, Y.; Huang, J. Facile and Green Synthesis of Titanate Nanotube/Graphene Nanocomposites for Photocatalytic H_2 Generation from Water. *Int. J. Hydrogen Energy* **2013**, *38*, 9178−9185.
(61) Tang, Y.; Gong, D.; Lai, Y.; Shen, Y.; Zhang, Y.; Huang, Y.; Tao, J.; Lin, C.; Dong, Z.; Chen, Z. Hierarchical Layered Titanate Microspherulite: Formation by Electrochemical Spark Discharge Spallation and Application in Aqueous Pollutant Treatment. *J. Mater. Chem.* **2010**, *20*, 10169−10178.
(62) Turki, A.; Kochkar, H.; Guillard, C.; Berhault, G.; Ghorbel, A. Effect of Na Contents and Thermal Treatment of Titanate Nanotubes on the Photocatalytic Degradation of Formic Acid. *Appl. Catal., B* **2013**, *138*−*139*, 401−415.
(63) Murakami, N.; Khurihara, Y.; Tsubota, T.; Ohno, T. Shape Controlled Anatase Titanium(IV) Oxide Particles Prepared by Hydrotehrmal Treatment of Peroxo Titanic Acid in the Presence of Polyvinyl Alcochol. *J. Phys. Chem. C* **2009**, *113*, 3062−3069.
(64) Furube, A.; Asahi, T.; Masuhara, H.; Yamashita, H.; Anpo, M. Charge Carrier Dynamics of Standard TiO_2 Catalysts Revealed by Femtosecond Diffuse Reflectance Spectroscopy. *J. Phys. Chem. B* **1999**, *103*, 3120−3127.
(65) Galinska, A.; Walendziewski, J. Photocatalytic Water Splitting over Pt-TiO_2 in the Presence of Sacrificial Reagents. *Energy Fuels* **2005**, *19*, 1143−1147.
(66) Kandiel, T. A.; Ivanova, I.; Bahnemann, D. W. Long-Term Investigation of the Photocatalytic Hydrogen Production on Platinized TiO_2: An Isotopic Study. *Energy Environ. Sci.* **2014**, *7*, 1420−1425.